JOURNAL OF MATERIALS SCIENCE 24 (1989) 187-191

Thickness dependence of electrical properties in thin films of undoped indium oxide prepared by ion-beam sputtering

T. SUZUKI, T. YAMAZAKI, M. TAKIZAWA , O. KAWASAKI
Department of Industrial Chemistry, Faculty of Technology, Tokyo University of Agriculture and Technology, Koganei, Tokyo 184, Japan

Preparation and electrical characterization of undoped indium oxide films were examined as a function of thickness and annealing. Thin films ranging from 1.1 to 113 nm thickness were deposited on glass substrates by ion-beam sputtering. Low-angle X-ray diffraction analysis in multi-layered films showed the possibility that physically continuous and almost flat films were formed even in the thinnest 1.1 nm films. Room temperature resistivity of as-deposited films decreased sharply by more than five orders of magnitude as the thickness increased from 1.1 to 5.2 nm. The 2.4 nm thick films, in its as-deposited state, showed a gradual resistivity modulation with the change of atmosphere between air and argon gas at room temperature. Annealing at 300° C for 5 h in air increased the resistivity drastically; the room temperature resistivity of 24.3 nm thick films changed from $2.2 \times 10^{-3}\,\Omega$cm (as-deposited) to higher than $\sim 10^5\,\Omega$cm (annealed).

1. Introduction

The opto-electrical properties of indium tin oxide (ITO) have been extensively studied for their application as transparent electrode and solar transmitting and heat-reflecting coatings on energy efficient windows [1, 2]. The ITO film usually consists of the indium oxide matrix and the dopant tin oxide of less than 10 mol %. In the course of the ITO formation from the indium oxide/tin oxide multi-layered films [3], we felt it necessary to elucidate separately the role of the undoped indium oxide film and of the tin oxide. As for the tin oxide film, a strong thickness dependence of electrical properties has already been reported [4–6]. Therefore, the present paper deals with the properties in undoped indium oxide films. Films thicker than about 50 nm have been prepared in a variety of techniques such as sputtering [7, 8], reactive evaporation [9–11], spray pyrolysis [12], evaporation of metal indium and the subsequent oxidation [13], chemical vapour deposition [14] and ion plating [15]. These films generally behave as if they were thickness independent. While the electrical properties of films thinner than 50 to 10 nm are reported to be thickness dependent. Ovadyahu *et al.* [16] have deposited samples on a microscope glass-slide by thermal evaporation and observed that the resistivity of films thinner than about 10 nm was thickness dependent. They postulated that this was due to the physical discontinuity in these films. Laser [17] has demonstrated the conductivity modulation by oxygen pressure variation in 10 to 40 nm thick crystalline films deposited on glasses by reactive evaporation; the relative conductivity change diminished as the film thickness increased. Pan and Ma [18, 19] have deposited a film on a microscope cover glass-slide kept at a temperature range of 320 to 350° C and measured the sheet resistance as a function of thickness during the growth of the film in a vacuum chamber. A sharp decrease in resistance by more than five orders of magnitude occurred at first as the thickness increased to about 30 nm and then the resistance decreased gradually with the thickness from about 50 to 270 nm. Electrical properties of films are greatly influenced not only by thickness but also by annealing [9, 20].

For example, Mizuhashi [20] has deposited films (35 to 60 nm thick) on glass substrates by evaporation and found that heat treatment at 500° C for 10 min drastically increased the resistivity by more than four orders of magnitude which was thought to be caused by the decrease in oxygen vacancies due to oxidation. In none of these investigations, were the effects of film thickness down to the order of 1 nm studied systematically.

Thus, as with our previous works on tin oxide films [4–6] we describe here that the electrical properties in thin films of undoped indium oxide are critically dependent on thickness and also on post-deposition annealing.

2. Experimental methods

An ion-beam sputtering (IBS) apparatus was used to sputter deposit thin films of indium oxide and multi-layered films of indium oxide/tin oxide from the sintered discs of In_2O_3 (99.99% pure) and SnO_2 (99.99% pure). Optical flat Pyrex glasses were used as substrates. Prior to mounting, the substrates were washed with acetone. The sputtering was done in a diffusion pump vacuum system. After the preset

0022-2461/89 $03.00 + .12 © 1989 Chapman and Hall Ltd.

vacuum (< 2 × 10^{-5} Torr) was reached, argon gas of purity 99.9995% was leaked into the discharge chamber and the total gas pressure during sputtering was maintained at 1 × 10^{-4} Torr. The 1.5 cm diameter ion source was operated at an ion-beam energy of 1000 eV and an accelerator voltage of 150 V. The temperatures of the substrate and the target did not exceed 90 and 130° C respectively, during sputtering shorter than 3 h. For further details of the IBS system, see [21] and [22].

Electrical measurements were made parallel to the interface on samples that were shaped (using masks) into two different configurations; one for the two prove method with an electrode gap of 0.5 mm wide × 8 mm long and the other for the Van der Pauw method on disc-films of 5 mm diameter. In the latter method, the Hall effect measurements were made under a d.c. magnetic field of 5500 Gauss. Platinum electrodes were formed by the IBS method. The deposition rate of the undoped indium oxide was determined by the thickness analysis of In_2O_3/SnO_2 multilayered films using a surface texture measuring instrument (Ferfcom, Tokyo Precision) and an X-ray diffractometer (RAD-B, Rigaku, Tokyo) with Ni-filtered Cu radiation at 30 KV and 20 mA. To form multi-layered films, the sputtering time for one tin oxide layer was set constant to 50 sec and that for one indium oxide layer varied from 50 to 1200 sec. The data for the low-angle X-ray diffraction intensity were collected with a scan speed of 0.2° min^{-1} and a step sampling of 0.002° in 2θ. The post-deposition annealing was carried out in air in an electric furnace. As-deposited films were annealed at 100° C for 5 h at first and then at 200° C for 5 h and finally at 300° C for 5 h.

3. Results and discussion

3.1. Film thickness and structure

The formation of indium oxide/tin oxide multilayered films was undertaken at first to verify (i) the deposition rate of the undoped indium oxide was independent of the sputtering time even at very short period of time and (ii) physically continuous and flat films of undoped indium oxide of the order of 1 nm thickness could be prepared. Fig. 1 shows typical examples of the low-angle X-ray diffraction patterns of multi-layered films. The thickness of one In_2O_3/SnO_2 pair, d, can be obtained from the Bragg equation:

$$d_n = \frac{n\lambda}{2 \sin \theta_n} \quad (1)$$

where n is the integer, λ is the wave length of X-ray (0.154 nm) and θ_n is the diffraction angle from the n-th reflection. Equation 1 can be rewritten as:

$$d_{n,n+1} = \frac{\lambda}{2}\left(\frac{2n+1}{\sin^2\theta_{n+1} - \sin^2\theta_n}\right)^{1/2} \quad (2)$$

A diffraction peak on the chart could be finally identified as resulting from a n-th reflection using, at first, the rough deposition rate of In_2O_3 and SnO_2 obtained from the sputtering time and the total film thickness given by the surface texture measuring instrument. Multi-layered films of the two shortest pair thicknesses, In_2O_3 (50 sec)/SnO_2 (50 sec) × 40 pairs and In_2O_3 (100 sec)/SnO_2 (50 sec) × 30 pairs, showed only the first (n = 1) satellite and thus the pair thickness was calculated from Equation 1. Other films, In_2O_3 (200 sec)/SnO_2 (50 sec) × 18 pairs, In_2O_3 (400 sec)/SnO_2 (50 sec) × 10 pairs, In_2O_3 (600 sec)/SnO_2 (50 sec) × 8 pairs, In_2O_3 (800 sec)/SnO_2 (50 sec) × 6 pairs, In_2O_3 (1000 sec)/SnO_2 (50 sec) × 5 pairs and In_2O_3 (1200 sec)/SnO_2 (50 sec) × 5 pairs, showed higher order ($n \geqslant 2$) satellite peaks and their pair thicknesses were determined using Equation 2. The pair thicknesses thus obtained are plotted in Fig. 2 as a function of the sputteri g time of the indium oxide. The plot is approximately linear and this clearly indicates that the deposition rate of the indium oxide is constant so long as the sputtering time is longer than 50 sec.

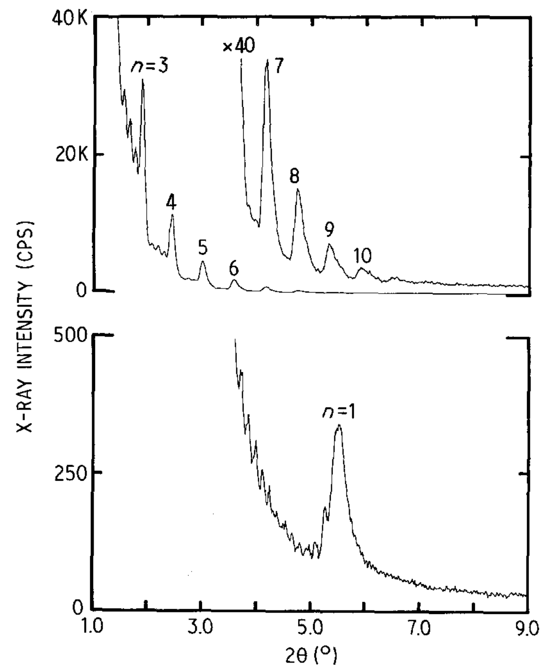

Figure 1 Typical patterns of low-angle X-ray diffraction intensity in In_2O_3/SnO_2 multi-layered films. Top graph – In_2O_3, 1200 sec; SnO_2, 50 sec; 5pairs. Bottom graph – In_2O_3, 50 sec; SnO_2, 50 sec; 40 pairs.

The gradient of the straight line, derived from the least square method, showed the deposition rate of the indium oxide to be 0.0113 nm sec^{-1}. The fact that the multi-layered film with the shortest designed pair thickness d = 1.44 nm, i.e. In_2O_3 (0.57 nm)/

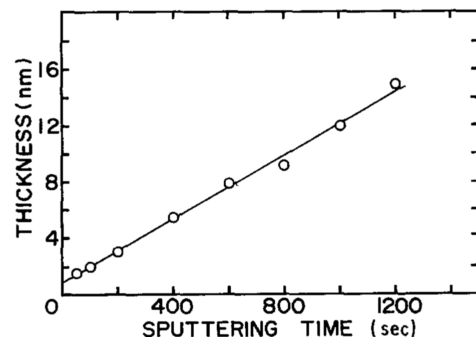

Figure 2 Thickness of one In_2O_3/SnO_2 pair as a function of sputtering time of one indium oxide layer. Sputtering time of one tin oxide layer is always 50 sec.

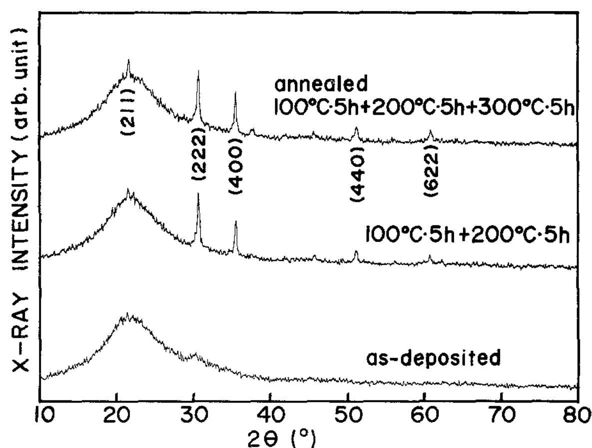

Figure 3 X-ray diffraction diagrams of 113 nm thick indium oxide film annealed under various conditions.

SnO_2 (0.87 nm) × 40 pairs, showed the first satellite (Fig. 1) indicated that approximately sinusoidal concentration distribution existed along the film thickness [23]. This in turn demonstrated the possibility of forming a physically continuous and almost flat film of indium oxide single layer as thin as ~0.6 nm. It is to be noted that the lattice constant of the cubic structure is 1.01 nm (JCPDS 6-0416). For films thicker than 2 to 3 nm, it is probable that these films are flat and smooth, because a higher order satellite ($n \geq 2$) appeared in multi-layered films such as In_2O_3 (2.26 nm)/SnO_2 (0.87 nm) × 18 pairs and In_2O_3 (4.56 nm)/SnO_2 (0.87 nm) × 10 pairs etc. The formation of the ultra-thin flat films thus being ensured, indirect as it is, deposition of undoped indium oxide films was then undertaken. The sputtering time was set to 100, 215, 464, 1000, 2154, 4642 and 10000 sec and this corresponded to the film thickness of 1.1, 2.4, 5.2, 11.3, 24.3, 52.5 and 113 nm, respectively. The structural analysis was performed on the 113 nm thick film in as-deposited and annealed state. Fig. 3 shows the X-ray diffraction diagrams which revealed that the as-deposited film was amorphous (or microcrystalline) and that the thermal crystallization led to a cubic structure (JCPDS 6-0416) with a slight tendency of preferred (400) growth. Annealing at 100° C for 5 h had no significant effect on the X-ray structure; the diffraction pattern remained the same as that of the as-deposited film. It is to be noted that the deposition rate varied very slowly due, probably, to the tungsten oxide film formation on the inside wall of the anode cylinder, deposition of sputtered particles on the accelerator grid, uneven target surface made by long time sputtering with 21 beamlets not uniformly mixed etc. Thus the deposition rate has always been measured just prior to the sample formation so that a designed film thickness might be surely realized.

3.2. Electrical properties

We observed a noticeable reduction in resistance after the sample was taken out of the vacuum chamber into air for films thinner than 24.3 nm, however no such change occurred in films thicker than 52.5 nm. Therefore, electrical measurements were carried out on stabilized samples which occurred approximately

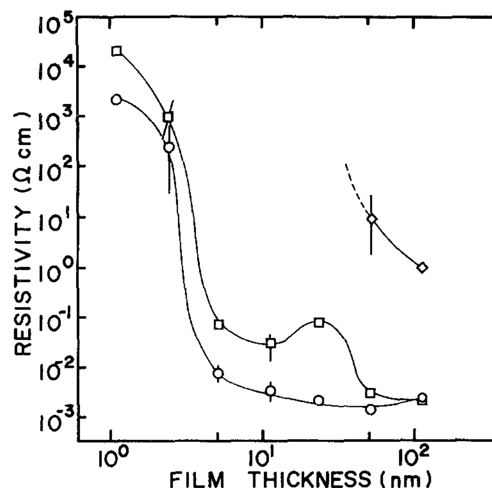

Figure 4 Room temperature resistivity as a function of film thickness and annealing for In_2O_3. As-deposited (○), annealed 100° C · 5 h + 200° C · 5 h (□), 100° C · 5 h + 200° C · 5 h + 300° C · 5 h (◇). The thickness from left to right is 1.1, 2.4, 5.2, 11.3, 24.3, 52.5 and 113 nm, respectively.

one day after the thin films were exposed in air. Room temperature electrical properties in air were measured both with the Van der Pauw method and the two prove method for films with relatively low resistivities ($< 10^{-1}$ Ω cm), while those of higher resistivities could be measured only with the two prove method. Values obtained from the two methods agreed within the experimental error. The variation in the room temperature resistivity with thickness on annealing is given in Fig. 4. Each plot indicates the averaged value and its deviation in four samples except that of the 1.1 nm thick film of two samples. Fig. 5 shows the room temperature Hall mobility and carrier (electron) density in relation to thickness and annealing. As-deposited amorphous films exhibits a sharp decrease in resistivity by more than five orders of magnitude as the thickness increases from 1.1 to 5.2 nm; above 24.3 nm the resistivity remained almost constant ($\sim 2 \times 10^{-3}$ Ω cm).

A similar observation was reported by Pan and Ma [18, 19], however, their measurements were made on a polycrystalline film at 320 to 350° C in the vacuum with an oxygen partial pressure from about 5×10^{-5} to 2×10^{-4} Torr. Another interesting feature in

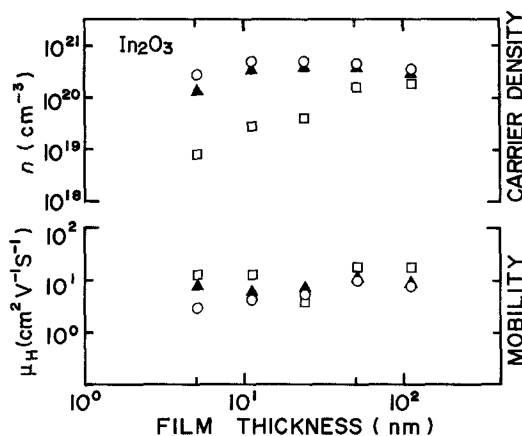

Figure 5 Room temperature carrier (electron) density and Hall mobility as a function of film thickness and annealing. As-deposited (○), annealed 100° C · 5 h (▲), 100° C · 5 h + 200° C · 5 h (□).

as-deposited amorphous films is the resistivity modulation by oxygen pressure variation as reported by Laser [17]. In our preliminary experiments, the resistivity modulation was observed at room temperature only in 2.4 nm thick as-deposited (amorphous) films; no other films (including 1.1 nm thick film) showed such an observable resistivity modulation. Room temperature resistivity of 2.4 nm thick films decreased gradually when transferred from air into ordinary argon gas of $\sim 1 \times 10^{-2}$ Torr oxygen partial pressure. The value changed reversibly from 2.5×10^2 (air) to 4.1 (argon, 30 min) and further down to $3.0 \times 10^{-1}\ \Omega$cm (argon, 15 h). A similar observation was reported in our previous work [5] in which ultra-thin tin oxide films (≤ 5 nm) showed no hydrogen gas sensitivity in the amorphous state at 150° C, while films around 10 nm or thicker showed a strong thickness dependence of sensitivity. Resistivity of films annealed at 100° C for 5 h are not given in Fig. 4 for simplicity, because they coincided with those of as-deposited when thicker than 5.2 nm, while thinner films showed slightly higher resistivities than those annealed at 100° C · 5 h + 200° C · 5 h.

As-deposited and annealed (100° C · 5 h) films thicker than 5.2 nm apparently showed the same X-ray structure (amorphous) and the same resistivity. However, Fig. 5 indicates further that annealing induced a relaxation in microstructure leading to an increased mobility which cancelled out the effect of reduced carrier density on the resistivity. The lowest resistivity of all films examined here was found in a 52.5 nm thick as-deposited film; it was $1.3 \times 10^{-3}\ \Omega$ cm with the Hall mobility of $12\ cm^2\ V^{-1}\ s^{-1}$ and the carrier density of $4.1 \times 10^{20}\ cm^{-3}$. Crystallization occurred during the subsequent annealing at 200° C for 5 h (Fig. 3) and this made the resistivity of the crystalline films higher by approximately one order of magnitude compared with the original amorphous films except the two thickest films. This increase is governed mainly by the reduction of carrier density, at least for 5.2, 11.3 and 24.3 nm thick films. Occurrence of resistivity maximum at 24.3 nm is due to the relative reduction in both carrier concentration and mobility; the latter in particular shows a peculiar behaviour compared with those of other films.

We have already reported a similar phenomenon in polycrystalline tin oxide films of about 50 nm thickness at 150 to 350° C [6]. There it was postulated that the resistivity maximum resulted from the combination of grain boundary resistance and the depletion region due to the chemisorption of oxygen atoms. Although detailed studies are needed for this point, no further investigation was made here. Further annealing at 300° C for 5 h made a progressive crystal growth (Fig. 3) and the resistivity became too high to be measured by the Van der Pauw method even in the thickest films. The 24.3 nm thick films showed higher resistivity than $\sim 10^5\ \Omega$cm and no reliable value was obtained. This drastic increase in resistivity is probably due to annihilation of oxygen vacancies due to oxidation during annealing in air was reported by Mizuhashi [20].

4. Conclusions

1. Undoped indium oxide films from 1.1 to 113 nm thickness were deposited on Pyrex glass substrates by ion-beam sputtering.

2. Room temperature resistivity of as-deposited films decreased sharply by more than five orders of magnitude as the thickness increased from 1.1 to 5.2 nm; above 24.3 nm the resistivity remained almost constant ($\sim 2 \times 10^{-3}\ \Omega$cm).

3. Room temperature resistivity of 2.4 nm thick films in as-deposited state decreased gradually when transferred from air into argon gas; the value changed from 2.5×10^2 (air) to $3.0 \times 10^{-1}\ \Omega$cm (argon, 15 h).

4. The 113 nm thick film was amorphous (or microcrystalline) in its as-deposited and annealed (100° C 5 h) state, while further annealing at 200° C for 5 h induced a crystallization to the cubic structure.

5. Room temperature resistivity increased with the crystallization at 200° C and this was mainly governed by the reduced electron density at least between the thickness range from 5.2 to 24.3 nm; the Hall mobility remained almost constant.

6. Further annealing at 300° C for 5 h made a progressive crystal growth and the resistivity increased drastically; the value of 24.3 nm thick film, $2.2 \times 10^{-3}\ \Omega$cm in an as-deposited state, became higher than $\sim 10^5\ \Omega$cm.

Acknowledgement

We thank Professor N. Oyama of the Department of Applied Chemistry for Resources for help in film thickness analysis.

References

1. K. L. CHOPRA, S. MAJOR and D. K. PANDY, *Thin Solid Films* **102** (1983) 1.
2. I. HAMBERG and C. G. GRANQUIST, *J. Appl. Phys.* **60** (1986) R123.
3. T. SUZUKI, T. YAMAZAKI and H. ODA, *J. Mater. Sci.* **23** (1988) 3026.
4. T. SUZUKI and T. YAMAZAKI, *J. Mater. Sci. Lett.* **6** (1987) 1086.
5. T. SUZUKI, T. YAMAZAKI, H. YOSHIOKA and K. HIKICHI, *J. Mater. Sci.* **23** (1988) 145.
6. T. SUZUKI, T. YAMAZAKI, H. YOSHIOKA and K. HIKICHI, *ibid.* **23** (1988) 1106.
7. L. C. SCHUMACHER, S. M-AFARA and M. J. DIGNAM, *J. Electrochem. Soc.* **133** (1986) 716.
8. H. K. MULLER, *Phys. Stat. Sol.* **27** (1968) 723.
9. A. GUPTA, P. GUPTA and V. K. SRIVASTAVA, *Thin Solid Films* **123** (1985) 325.
10. P. NATH and R. F. BUNSHAH, *ibid.* **69** (1980) 63.
11. S. NOGUCHI and H. SAKATA, *J. Phys. D: Appl. Phys.* **13** (1980) 1129.
12. W. SIEFERT, *Thin Solid Films* **120** (1984) 275.
13. K. B. SUNDARAM and G. K. BHAGAVAT, *Phys. Stat. Sol.* (*a*) **63** (1981) K15.
14. A. P. MAMMANA, E. S. BRAGA, I. TORRIANI and R. L. ANDERSON, *Thin Solid Films* **85** (1981) 355.
15. R. P. HOWSON, J. N. AVARITSIOTIS, M. I. RIDGE and C. A. BISHOP *ibid.* **58** (1979) 379.
16. Z. OVADYAHU, B. OVRYN and H. W. KRANER, *J. Electrochem. Soc.* **130** (1983) 917.
17. D. LASER, *J. Appl. Phys.* **52** (1981) 5179.
18. C. A. PAN and T. P. MA, *J. Electrochem. Soc.* **128** (1981) 1953.
19. C. A. PAN and T. P. MA, *Appl. Phys. Lett.* **37** (1980) 163.

20. M. MIZUHASHI, *Thin Solid Films* **70** (1980) 91.
21. T. SUZUKI, T. YAMAZAKI, H. YOSHIOKA, K. TAKAHASHI and T. KAGEYAMA, *J. Mater. Sci. Lett.* **6** (1987) 437.
22. T. SUZUKI, T. YAMAZAKI, K. TAKAHASHI, T. KAGEYAMA and H. ODA, *ibid.* **7** (1988) 79.
23. J. DUMOND and J. P. YOUTZ, *J. Appl. Phys.* **11** (1940) 357.

Received 1 January
and accepted 9 May 1988